Turkish Journal of Chemistry

http://journals.tubitak.gov.tr/chem/

Research Article

Turk J Chem
(2014) 38: 994 – 1005

doi:10.3906/kim-1407-26

Electrochemistry of Fe(IV) and Mn(IV) corroles containing *meso*-dichlorophenyl substituents and the use of these compounds as catalysts for the electroreduction of dioxygen in acid media

Lina YE[1,2], Zhongping OU[2,*], Deying MENG[2], Mingzhu YUAN[2], Yuanyuan FANG[3], Karl M. KADISH[3,*]

[1]Computer College, Jilin Normal University, Siping, P. R. China
[2]School of Chemistry and Chemical Engineering, Jiangsu University, Zhenjiang, P. R. China
[3]Department of Chemistry, University of Houston, Houston, TX, USA

Received: 09.07.2014 • **Accepted:** 24.08.2014 • **Published Online:** 24.11.2014 • **Printed:** 22.12.2014

Abstract: Two *meso*-dichlorophenyl substituted metallocorroles were synthesized and characterized as to their electrochemical and spectroelectrochemical properties in dichloromethane, benzonitrile, and pyridine containing 0.1 M tetra-*n*-butylammonium perchlorate (TBAP) as supporting electrolyte. The examined compounds are represented as $(Cl_2Ph)_3CorFe^{IV}Cl$ and $(Cl_2Ph)_3CorMn^{IV}Cl$ where $(Cl_2Ph)_3Cor$ is the trianion of 5,10,15-tri(2,4-dichlorophenyl)corrole. Each metallocorrole was examined as to its catalytic activity for the electoreduction of dioxygen when coated on an edge-plane pyrolytic graphite electrode in 1.0 M $HClO_4$. Cyclic voltammetry combined with linear sweep voltammetry at a rotating disk electrode (RDE) and a rotating ring disk electrode (RRDE) was utilized to evaluate the catalytic activity for the electroreduction of O_2. The main O_2 reduction product is hydrogen peroxide under the given experimental conditions.

Key words: Metallocorroles, synthesis, electrochemistry, catalytic activity, dioxygen reduction

1. Introduction

Corroles and metallocorroles have attracted a great deal of interest[1–9] in part because of their potential applications as catalysts for a variety of reactions.[9–27] Our own research interests have long been focused on the synthesis and characterization of metallocorroles with an emphasis on cobalt,[16–19,28–33] iron,[34–36] and manganese derivatives.[37,38] In the present work, the synthesis, electrochemistry, and spectroelectrochemistry of iron(IV) and manganese(IV) *meso*-dichlorophenyl substituted metallocorroles are described. The examined compounds are represented as $(Cl_2Ph)_3CorFeCl$ and $(Cl_2Ph)_3CorMnCl$, where $(Cl_2Ph)_3Cor$ is the trianion of the 5,10,15-tri(2,4-dichlorophenyl)corrole. The structures of these compounds are shown in the Chart. Electrochemical and spectroelectrochemical properties of each corrole were examined in dichloromethane, benzonitrile, and pyridine containing 0.1 M TBAP as supporting electrolyte.

Metallocorroles with cobalt,[16,17,19–21,24,25,39] iron,[20,26] and manganese[20] central metal ions are able to catalyze the electroreduction of oxygen via a 2e transfer process to produce H_2O_2 or a 4e transfer process to generate H_2O. We have earlier examined numerous cobalt triarylcorroles[16,17,19,24,25] as to their catalytic properties for the reduction of O_2 and demonstrated that the type and position of substituents on the 3

*Correspondence: kkadish@uh.edu, zpou2003@yahoo.com

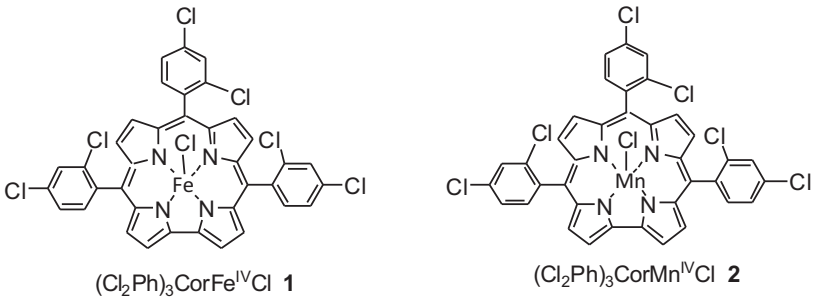

Chart. Structures of examined metallocorroles.

phenyl rings of a triarylcorrole will significantly affect the catalytic activity of these compounds towards the reduction of O_2.[24,25] We have also shown that a 2e reduction of O_2 exclusively occurs when using cobalt corrole catalysts with substituents on the *ortho*-positions of the phenyl rings; this is due to steric hindrance of the substituents, which can block dimerization of the corroles on the electrode surface.[24,25] However, it was not known if triarylcorroles containing manganese and iron central metal ions would be affected by steric hindrance of the phenyl ring substituents. This is addressed in the present work where 2 newly synthesized Mn(IV) and Fe(IV) corroles having bulky Cl substituents on the *ortho*-position of the phenyl rings are examined as to their catalytic activity for the electoreduction of O_2 at an edge-plane pyrolytic graphite electrode in 1.0 M $HClO_4$.

2. Results and discussion

2.1. UV-visible spectra

UV-visible spectra of $(Cl_2Ph)_3$CorFeCl **1** and $(Cl_2Ph)_3$CorMnCl **2** in CH_2Cl_2, PhCN, and pyridine are illustrated in Figure 1, while the absorption maxima and molar absorptivities of the compounds are summarized in Table 1. $(Cl_2Ph)_3$CorFeCl **1** has a split Soret band at 368 and 392 nm and 2 Q bands at 516 and 623 nm in CH_2Cl_2. Identical Soret and Q band absorption maxima are seen in PhCN for the same compound (Figure 1a; Table 1). These spectral features are similar to those for previously examined Fe(IV) triaryl-substituted corroles in CH_2Cl_2.[40] In contrast, only a single strong Soret band is observed for the related Fe(IV) corrole in pyridine. This band is located at 415 nm and is red-shifted by $\sim$20 nm in pyridine upon changing the solvent from CH_2Cl_2 or PhCN. This shift in λ_{max} is consistent with a coordination of pyridine at the central metal ion.

Table 1. UV-visible spectral data, λ_{max}, nm ($\varepsilon\times\ 10^{-4}$ M^{-1} cm^{-1}).

Compound	Solvent	Soret region			Visible region			
$(Cl_2Ph)_3$CorFeCl **1**	CH_2Cl_2	368 (3.6)	392 (3.7)		516 (0.6)	623 (0.2)		
	PhCN	369 (3.5)	396 (3.6)		516 (0.6)	623 (0.3)		
	pyridine	337 (1.7)	415 (4.7)		565 (0.9)	612 (0.8)	715 (0.2)	
$(Cl_2Ph)_3$CorMnCl **2**	CH_2Cl_2	314 (2.4)	359 (2.9)	416 (4.0)	593 (0.5)			
	PhCN	316 (2.3)	364 (2.7)	422 (3.9)	593 (0.5)			
	pyridine	319 (2.4)	405 (2.9)	435 (3.3)	499 (1.7)	549 (0.8)	585 (0.9)	661 (1.1)

Meso-triaryl-substituted Mn(IV) corroles are known to exhibit 3 well-defined Soret bands in CH_2Cl_2.[40] Similar spectral features are observed for $(Cl_2Ph)_3CorMn^{IV}Cl$ **2** in PhCN. As seen in Figure 1b and Table 1, the Soret band absorptions are located at 314, 359, and 416 nm in CH_2Cl_2 and 316, 364, and 422 nm in PhCN. There is also a single Q band at 593 nm in both solvents. However, a quite different spectrum is seen in pyridine,

where 4 Q bands are located at 499, 549, 585, and 661 nm (see Table 1) as compared to a single Q band at 593 nm in the other 2 solvents. The shape of the spectrum for $(Cl_2Ph)_3CorMn^{IV}Cl$ **2** in pyridine was previously assigned as belonging to a Mn(III) corrole,[37] and the data in Figure 1b suggest that $(Cl_2Ph)_3CorMn^{IV}Cl$ **2** has been reduced to its Mn(III) form in the pyridine solvent.

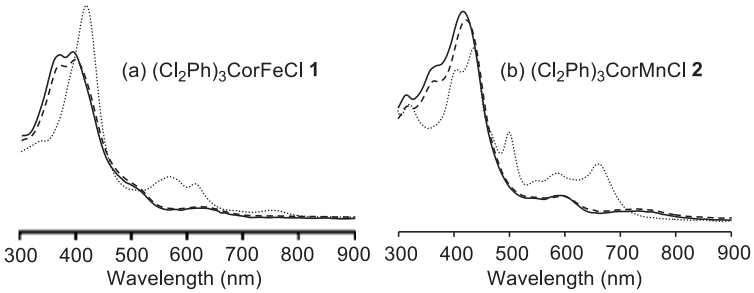

Figure 1. UV-visible spectra of the neutral compounds (a) $(Cl_2Ph)_3CorFeCl$ **1** and (b) $(Cl_2Ph)_3CorMnCl$ **2** in CH_2Cl_2 (—), PhCN (– – –), and pyridine (· · ·) containing 0.1 M TBAP.

2.2. Electrochemistry of $(Cl_2Ph)_3CorFe^{IV}Cl$ 1

Electrochemistry of the Fe(IV) corrole was carried out in CH_2Cl_2, PhCN, and pyridine containing 0.1 M TBAP and the resulting cyclic voltammograms are illustrated in Figure 2.

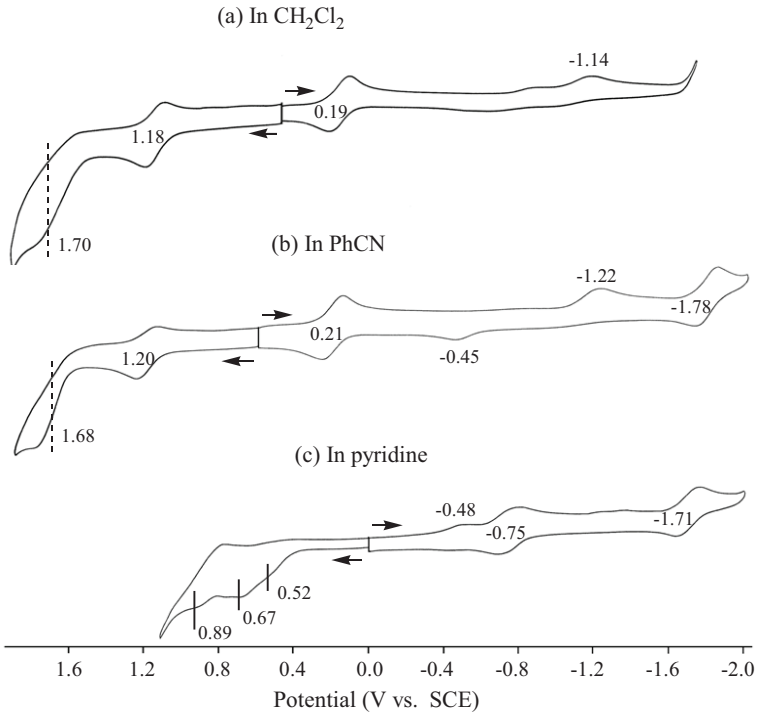

Figure 2. Cyclic voltammograms of $(Cl_2Ph)_3CorFeCl$ **1** in (a) CH_2Cl_2, (b) PhCN, and (c) pyridine containing 0.1 M TBAP.

Two reversible to quasi-reversible oxidations are observed at 1.18 and 1.70 V (in CH_2Cl_2, Figure 2a) or 1.20 and 1.68 V (in PhCN, Figure 2b). Similar oxidation behavior has been reported for other triaryl-

substituted iron(IV) corroles, where the first electron abstraction was proposed to occur at the conjugated corrole macrocycle.[40,41] However, thin-layer spectroelectrochemistry of $(Cl_2Ph)_3CorFeCl$ indicates that the Soret bands decrease only slightly in intensity after controlled potential oxidation at 1.50 V in PhCN (see Figure 3a) and this might suggest that the first one-electron abstraction of the Fe(IV) corrole is in part metal-centered. This is consistent with a proposal by Walker and coworkers who examined (OMC)$Fe^{IV}Cl$ (OMC is a trianion of the β-octamethylcorrole) and described the electronic state of the compound as an intermediate-spin Fe(III) corrole which was antiferromagnetically coupled to an OMC cation radical.[42]

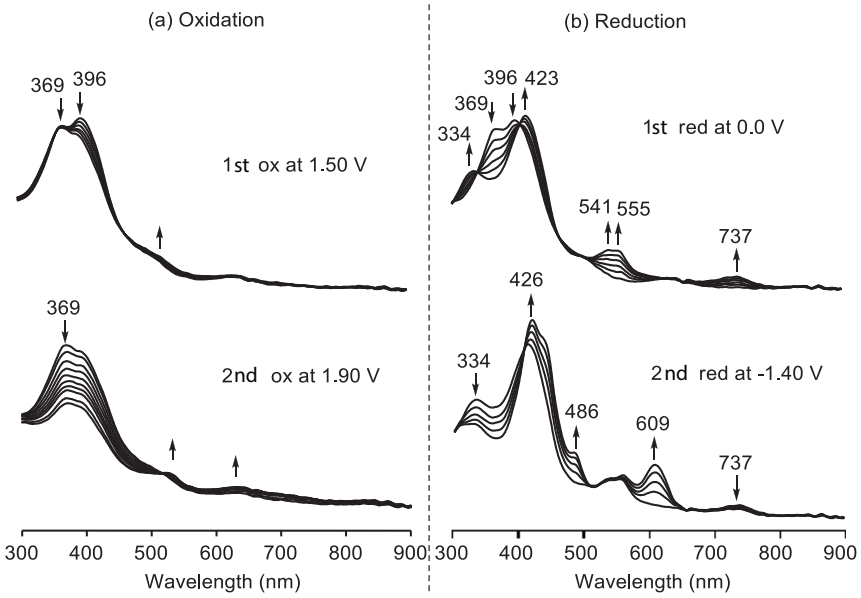

Figure 3. Thin-layer UV-visible spectral changes of $(Cl_2Ph)_3CorFeCl$ **1** during controlled potential oxidations (a) and reductions (b) in PhCN containing 0.1 M TBAP.

Significant spectral changes occurred during the second controlled potential oxidation of $(Cl_2Ph)_3CorFeCl$ when the potential was held at 1.90 V in PhCN (Figure 3a). The oxidation product exhibits a decreased intensity Soret band (at 369 nm) that indicates a macrocycle-centered electron transfer process under the given solution conditions.

$(Cl_2Ph)_3CorFe^{IV}Cl$ also exhibits 2 reductions at 0.19 and –1.14 V in CH_2Cl_2, while 3 reductions are seen for the same compound at $E_{1/2}$ = 0.21, E_{pc} = –1.22, and $E_{1/2}$ = –1.78 V in PhCN (Figure 2). The second reduction at E_{pc} = –1.22 V is coupled to a reoxidation peak at E_{pa} = –0.45 V. Based on the spectroelectrochemical data in Figure 3b, the first 2 reductions of $(Cl_2Ph)_3CorFe^{IV}Cl$ are assigned as metal-centered to stepwise give the Fe(III) and Fe(II) forms of the corrole.

$(Cl_2Ph)_3CorFe^{IV}Cl$ undergoes 3 reductions in pyridine, which are located at E_{pc} = –0.48, $E_{1/2}$ = –0.75, and $E_{1/2}$ = –1.71 V. The first reduction is irreversible and has a relatively small peak current as compared to the second and third reductions (see Figure 2c). All 3 reductions of $(Cl_2Ph)_3CorFe^{IV}Cl$ are proposed to occur at the metal center as described in the Scheme, where the initial Fe(IV) corrole in pyridine is proposed to exist in an equilibrium between $(Cl_2Ph)_3CorFe^{IV}(py)Cl$ and $[(Cl_2Ph)_3CorFe^{IV}(py)]^+$. The lower peak current for the first reduction of $[(Cl_2Ph)_3CorFe^{IV}(py)]^+$ at –0.48 V would indicate that only a small amount of this

species exists in solution. The same Fe(III) corrole is formed after reduction at –0.48 or –0.75 V and this species is then reversibly reduced at a more negative potential of –1.71 V to give the Fe(II) corrole in pyridine.

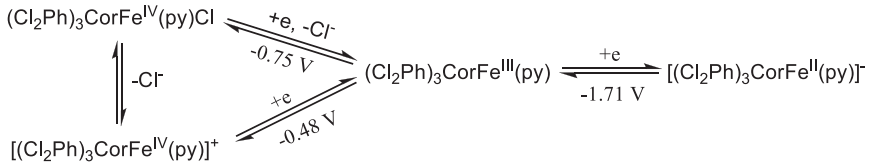

Scheme. Proposed reduction mechanism of cpd **1** in pyridine.

3. Electrochemistry of $(Cl_2Ph)_3CorMn^{IV}Cl$ 2

Cyclic voltammograms of Mn(IV) corrole in CH_2Cl_2 and PhCN containing 0.1 M TBAP are shown in Figure 4. The first reversible one-electron reduction is located at $E_{1/2}$ = 0.24 V in CH_2Cl_2 and 0.25 V in PhCN. The second reduction is also reversible and located at $E_{1/2}$ = –1.40 V in PhCN. However, this process is not reversible in CH_2Cl_2, where a chemical reaction is coupled with the electron transfer process. The UV-visible spectral changes obtained during the 2 reductions of $(Cl_2Ph)_3CorMn^{IV}Cl$ are given in Figure 5a and indicate that Mn(III) and Mn(II) corroles are generated upon the 2 stepwise electroreductions of **2** in PhCN containing 0.1 M TBAP.

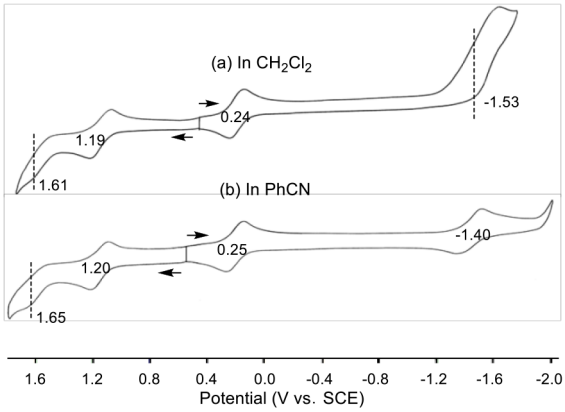

Figure 4. Cyclic voltammograms of $(Cl_2Ph)_3CorMnCl$ **2** in (a) CH_2Cl_2 and (b) PhCN containing 0.1 M TBAP.

$(Cl_2Ph)_3CorMnCl$ **2** undergoes 2 reversible 1-electron oxidations in CH_2Cl_2 and PhCN. The first is located at $E_{1/2}$ = ~1.19 V and the second at $E_{1/2}$ = 1.61 to 1.65 V (see Figure 4). The UV-visible spectral changes during these 2 oxidations are shown in Figure 5b and are consistent with formation of a Mn(IV) π-cation radical and Mn(IV) dication rather than with formation of a Mn(V) corrole after the 2 stepwise 1-electron abstractions.

A summary of potentials for reduction and oxidation of $(Cl_2Ph)_3CorFeCl$ **1** and $(Cl_2Ph)_3CorMnCl$ **2** is given in Table 2, which also includes data on related Fe(IV) and Mn(IV) corroles.

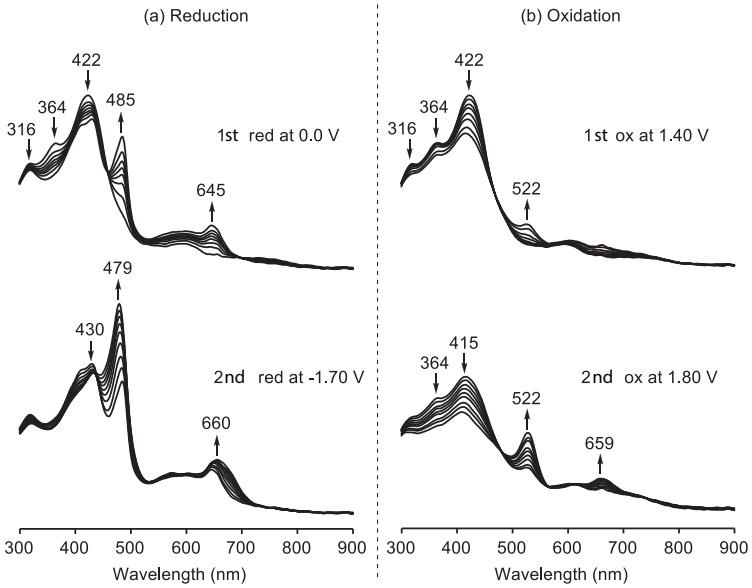

Figure 5. Thin-layer UV-visible spectral changes of $(Cl_2Ph)_3CorMnCl$ **2** during controlled potential reduction and oxidation in PhCN containing 0.1 M TBAP.

Table 2. Half-wave potentials (V vs. SCE) of cpds **1** and **2** in different solvents containing 0.1 M TBAP.

Solvent	Compound	Oxidation		Reduction			Ref
		2nd	1st	1st	2nd	3rd	
CH_2Cl_2	$(Cl_2Ph)_3CorFe^{IV}Cl$ **1**	1.70	1.18	0.19	–1.14[a]		*tw*
	$(p\text{-}CF_3Ph)_3CorFe^{IV}Cl$		1.18	0.19	–1.20[a]		39
	$(Ph)_3CorFe^{IV}Cl$		1.07	0.05	–1.25[a]		39
	$(p\text{-}CH_3Ph)_3CorFe^{IV}Cl$		1.02	0.03	–1.26[a]		39
PhCN	$(Cl_2Ph)_3CorFe^{IV}Cl$ **1**	1.68	1.20	0.21	–1.22[a]	–1.78	*tw*
py	$(Cl_2Ph)_3CorFe^{IV}Cl$ **1**	0.89[b]	0.52[a]	–0.48[a]	–0.75	–1.71	*tw*
CH_2Cl_2	$(Cl_2Ph)_3CorMn^{IV}Cl$ **2**	1.61	1.19	0.24	–1.53		*tw*
	$(p\text{-}CF_3Ph)_3CorMn^{IV}Cl$		1.15	0.23			39
	$(Ph)_3CorMn^{IV}Cl$		1.03	0.09			39
	$(p\text{-}CH_3Ph)_3CorMn^{IV}Cl$		0.97	0.07			39
PhCN	$(Cl_2Ph)_3CorMn^{IV}Cl$ **2**	1.65	1.20	0.25	–1.40		*tw*

[a] Irreversible peak potential at a scan rate of 0.10 V/s. [b] An irreversible peak can also be seen at $E_{pa} = 0.67$ V.

3.1. Electrocatalytic reduction of O_2

Figure 6 illustrates the cyclic voltammograms of the $(Cl_2Ph)_3CorFeCl$ **1** and $(Cl_2Ph)_3CorMnCl$ **2** adsorbed on an EPPG disk electrode in 1.0 M $HClO_4$ under N_2 (dashed line) and under air (solid line). A surface reaction indicated by an asterisk is seen at about 0.4 V. No other peak is seen for cpd **1** under N_2 but a broad peak at 0.10 V with a low current is exhibited by cpd **2** under the same experimental conditions. The current–voltage curve in 1.0 M $HClO_4$ under air shows a large cathodic reduction peak for both compounds, at $E_{pc} = 0.10$ V for cpd **1** and 0.13 V for cpd **2** at a scan rate of 50 mV/s. As will be shown, the cathodic (reduction) peaks in air-saturated $HClO_4$ correspond to the catalytic reduction of dissolved O_2 to give almost exclusively H_2O_2.

The dioxygen in solution is also reduced at a bare EPPG electrode without the corrole but this reduction occurs at a more negative potential of E_{pc} = –0.13 V for a scan rate of 50 mV/s.[25]

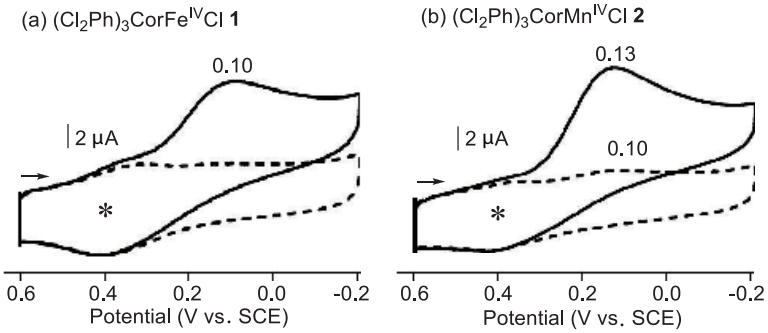

Figure 6. Cyclic voltammograms of corroles **1** and **2** absorbed on an EPPG electrode in 1.0 M $HClO_4$ under N_2 (– – –) and under air (—). Scan rate = 50 mV/s.

Peak potentials for the catalytic reduction of dioxygen at the corrole coated electrodes are almost the same as those for the Fe(IV) and Mn(IV) corroles in acid media under air, which indicates that this reaction is not strongly influenced by differences in the central metal ion.

The catalytic reduction of O_2 was also monitored using a rotating disk electrode (RDE) to calculate the number of electrons transferred. The RDE response was similar for both corroles in air-saturated 1.0 M $HClO_4$ and is characterized by a half-wave potential located at almost identical potentials of 0.21 for **1** and 0.22 V for **2**, where i_{max} is the limiting current measured at –0.05 V for a rotation rate of 400 rpm and $E_{1/2}$ is the potential when $i = 0.5 i_{max}$ (Figure 7).

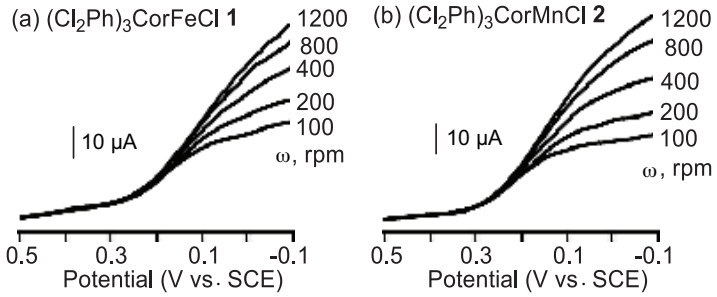

Figure 7. Current–voltage curve for catalytic reduction of O_2 in 1.0 M $HClO_4$ saturated with air at a rotating EPPG disk electrode coated with (a) $(Cl_2Ph)_3CorFeCl$ **1** and (b) $(Cl_2Ph)_3CorMnCl$ **2**. The electrode rotating rates (ω) are indicated on each curve. Potential scan rate = 50 mV/s.

The number of electrons transferred during reduction of dioxygen was calculated from the magnitude of the steady-state limiting currents, which were taken at a fixed potential of –0.05 V on the plateau of the catalytic wave in Figure 7. When the amount of O_2 reduction at the corrole modified electrode is controlled by mass transport alone, the relationship between the limiting current and rotation rate can be defined by the Levich equation.[43]

$$J_{lev} = 0.62nFAD^{2/3}cv^{-1/6}\omega^{1/2}, \quad (1)$$

where n is the number of electrons transferred in the overall electrode reaction, F *is* the Faraday constant (96485 C mol^{-1}), A is the electrode area (cm^2), D is the dioxygen diffusion coefficient (cm^2 s^{-1}), c is the

bulk concentration of O_2 in 1.0 M $HClO_4$, v is the kinematic viscosity of the solution, and ω is the angular rotation rate of the electrode (rad s^{-1}).

Plots of the reciprocal limiting current density vs. the reciprocal of the square root of the rotation rate (Figure 8) result in a straight line that obeys the Koutecky–Levich equation, where j is the measured limiting current density (mA cm^{-2}), j_{lev} is the Levich current, and j_k is the kinetic current, which can be obtained experimentally from the intercept of the Koutecky–Levich line in Figure 8.

$$1/j = 1/j_{lev} + 1/j_k \tag{2}$$

$$j_k = 10^3 knF\Gamma c \tag{3}$$

The value of $k(M^{-1}\ s^{-1})$ in Eqs. (2) and (3) is the second-order rate constant of the reaction that limits the plateau current and Γ(mol cm^{-2}) is the surface concentration of the catalyst. The other terms in Eq. (3) have their usual significance as described previously. The slope of a plot in Figure 8 obtained by linear regression can then be used to estimate the average number of electrons (n) involved in the catalytic reduction of O_2.[44] This analysis was carried out and the number of electrons transferred per dioxygen molecule (n) during the catalytic reduction of O_2 calculated for cpds **1** and **2**.

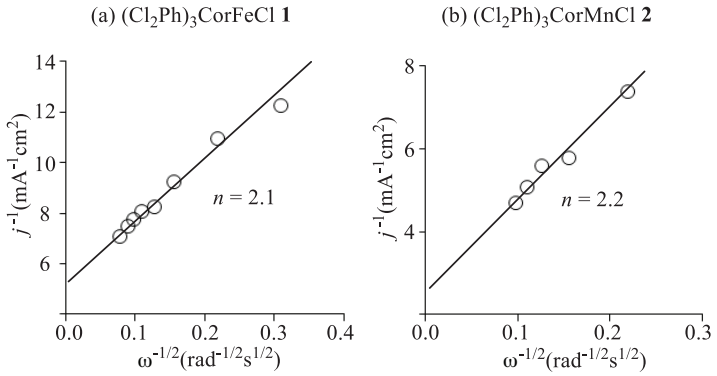

Figure 8. Koutecky–Levich plots for catalyzed reduction of O_2 in 1.0 M $HClO_4$ saturated with air at a rotating EPPG disk electrode coated with (a) $(Cl_2Ph)_3CorFeCl$ **1** and (b) $(Cl_2Ph)_3CorMnCl$ **2**.

A 2-electron transfer (n= 2) would generate 100% H_2O_2, while a 4-electron transfer (n = 4) would give 0% H_2O_2 and 100% H_2O. The Koutecky–Levich plots in Figure 8 show the number of electrons transferred (n) for compounds **1** and **2** to be 2.1 and 2.2, which corresponds to 95%–90% H_2O_2 produced. This indicates that the catalytic electroreduction of O_2 by **1** and **2** is a 2e transfer process, giving mainly H_2O_2 as a product rather than H_2O as a 4e transfer reduction product.

The catalytic reduction of O_2 was also examined at an RRDE under the same solution conditions. The disk potential was scanned from 0.5 to –0.1 V at a rotation speed of 200 rpm while holding the ring potential constant at 1.0 V. These data are shown in Figure 9, where the disk current begins to increase at about 0.30 V and a plateau is reached at about 0.10 V. The anodic ring current increases throughout the range of the disk potentials, where the disk current rises. The percentage of H_2O_2 is given by Eq. (4), where I_D and I_R are the Faradic currents at the disk and ring electrodes, respectively.

$$\%H_2O_2 = 100(2I_R/N)/(I_D + I_R/N) \tag{4}$$

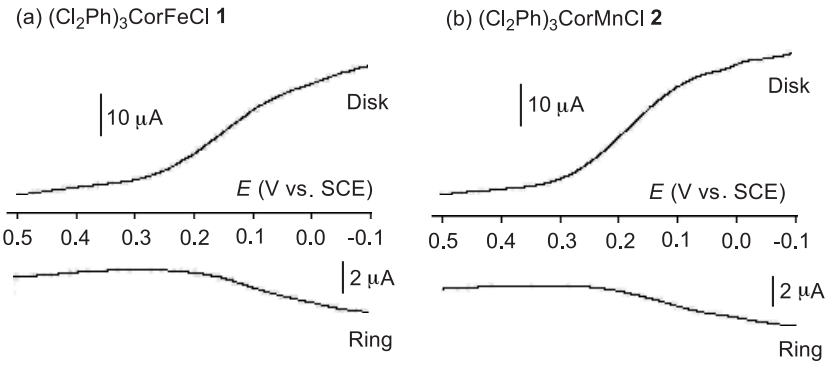

Figure 9. Rotating ring-disk electrode voltammograms of (a) $(Cl_2Ph)_3CorFeCl$ **1** and (b) $(Cl_2Ph)_3CorMnCl$ **2** in air saturated 1.0 M $HClO_4$ with the potential of the ring electrode maintained at 1.0 V. Rotation rate = 200 rpm and scan rate = 10 mV/s.

The intrinsic value of the collection efficiency (N) in Eq. (4) was determined to be 0.24 using the $[Fe(CN)_6]^{3-}/[Fe(CN)_6]^{4-}$ redox couple in 1.0 M KCl. The amount of H_2O_2 formed upon the reduction of dioxygen was calculated as 91% for compound **1** and 92% for compound **2** under the given experimental conditions. These values are similar to those calculated using the Koutecky–Levich plots in Figure 8.

It should be pointed out that an overall 4e transfer process to give H_2O as a product was previously reported in a pH 7 solution using iron tri(pentafluorophenyl)corrole, Fe(tpfc)Cl as the catalyst.[19] However, in the current study, H_2O_2 is the main product of dioxygen reduction in 1.0 M $HClO_4$. This is because the bulky *ortho*-Cl substituents on the *meso*-phenyl rings of the corrole can lead to steric hindrance, which can prevent the $\pi-\pi$ interactions between the macrocycles, thus hindering the formation of dimers on the electrode surface and preventing the occurrence of a 4-electron reduction to give an H_2O reduction product and an n value of 4.[24,45] A 2-electron transfer process ($n=2$) with only an H_2O_2 reduction product was also recently reported by using cobalt triphenylcorroles[23] or ferrocenyl-substituted cobalt porphyrins as catalysts.[46]

In conclusion, iron(IV) or Mn(IV) corroles containing a bulky substituent on the *meso*-position of the macrocycle can be utilized as a selective electrocatalyst for the 2e reduction of dioxygen to give H_2O_2 but not H_2O as a product in 1.0 M $HClO_4$.

4. Experimental

4.1. Chemicals

Dichloromethane (CH_2Cl_2), benzonitrile (PhCN), and pyridine (Py) were purchased from Sigma-Aldrich Co. and used as received for electrochemistry and spectroelectrochemistry experiments. Tetra-n-butylammonium perchlorate (TBAP) was purchased from Sigma Chemical or Fluka Chemika Co., recrystallized from ethyl alcohol, and dried under vacuum at 40 °C for at least 1 week prior to use.

$(Cl_2Ph)_3CorFeCl$ **1**. The free-base corrole $(Cl_2Ph)_3CorH_3$[47] (54.9 mg, 0.075 mmol) and $FeCl_2 \cdot 4H_2O$ (10 equivalents vs. the free-base corrole) were dissolved in pyridine and the mixture heated to reflux. After 30 min the mixture was diluted by $CHCl_3$ and washed twice with HCl (10%). After the organic phase turned from green to brown the product was washed with water. The organic layer was collected and evaporated to dryness. The sample was purified by chromatography on an Al_2O_3 column with CH_2Cl_2 as eluent. Yield 23%. UV-vis (PhCN): λ_{max}, nm, ($\varepsilon\times\ 10^{-4}$ $M^{-1}cm^{-1}$) 369 (3.5), 396 (3.6), 516 (0.6), 623 (0.3). MS (MALDI-TOF): m/z 786.365, calcd. for $[M\text{-}Cl]^+$ 786.121.

$(Cl_2Ph)_3CorMnCl$ **2**. The procedure for synthesis of cpd **2** is the same as described above for cpd **1**, but with 10 equivalents of $Mn(OAc)_2 \cdot 4H_2O$ utilized. The yield was 41%. UV-vis (PhCN): $\lambda_{max,}$ nm, ($\varepsilon \times 10^{-4}$ $M^{-1}cm^{-1}$) 316 (2.2), 364 (2.7), 422 (3.8), 593 (0.5). MS (MALDI-TOF): m/z 785.244, calcd. for $[M\text{-}Cl]^+$ 785.214.

4.2. Instrumentation

Cyclic voltammetry was carried out at 298 K using an EG&G Princeton Applied Research (PAR) 173 potentiostat/galvanostat or a Chi-730C Electrochemistry Work Station. A 3-electrode system was used for cyclic voltammetric measurements and rotating disk voltammetry. The working electrode was glassy carbon or graphite (Model MT134, Pine Instrument Co.) A platinum counter electrode and a homemade saturated calomel reference electrode (SCE) were also used. The SCE was separated from the bulk of the solution by a fritted glass bridge of low porosity that contained the solvent/supporting electrolyte mixture.

The RRDE was purchased from Pine Instrument Co. and consisted of a platinum ring and a removable edge-plane pyrolytic graphite (EPPG) disk (A = 0.196 cm^2). A Pine Instrument MSR speed controller was used for the RDE and RRDE experiments. The Pt ring was first polished with 0.05 micron α-alumina powder and then rinsed successively with water and acetone before being activated by cycling the potential between 1.20 and –0.20 V in 1.0 M $HClO_4$ until reproducible voltammograms were obtained.[48,49]

The corrole catalysts were irreversibly adsorbed on the electrode surface by means of a dip-coating procedure described in the literature.[16,45] The freshly polished electrode was dipped in a 1.0 mM catalyst solution of CH_2Cl_2 for 5 s, transferred rapidly to pure CH_2Cl_2 for 1–2 s, and then exposed to air where the adhering solvent rapidly evaporated, leaving the corrole catalyst adsorbed on the electrode surface. All experiments were carried out at room temperature.

Thin-layer UV-visible spectroelectrochemical experiments were performed with a home-built thin-layer cell that has a light transparent platinum net working electrode. Potentials were applied and monitored with an EG&G PAR Model 173 potentiostat. Time-resolved UV-visible spectra were recorded with a Hewlett-Packard Model 8453 diode array spectrophotometer. High purity N_2 from Trigas was used to deoxygenate the solution and kept over the solution during each electrochemical and spectroelectrochemical experiment.

Acknowledgments

This work was supported by grants from the Robert A. Welch Foundation (KMK, Grant E-680) and the Natural Science Foundation of China (Grant 21071067).

References

1. Erben, C.; Will, S.; Kadish, K. M. In *The Porphyrin Handbook*; Kadish, K. M.; Smith, K. M.; Guilard, R., Eds. Academic Press: New York, NY, USA, 2000, Vol. 2, pp. 233–300.
2. Paolesse, R. In *The Porphyrin Handbook*; Kadish, K. M.; Smith, K. M.; Guilard, R., Eds. Academic Press: San Diego, CA, USA, 2000, Vol. 2, pp. 201–232.
3. Gross, Z.; Gray, H. B. *Comm. Inorg. Chem.* **2006**, *27*, 61–72.
4. Aviv-Harel, I.; Gross, Z. *Chem., Eur. J.* **2009**, *15*, 8382–8394.
5. Gryko, D. T.; Fox, J. P.; Goldberg, D. P. *J. Porphyrins Phthalocyanines* **2004**, *8*, 1091–1105.
6. Guilard, R.; Barbe, J. M.; Stern, C.; Kadish, K. M. In *The Porphyrin Handbook*; Kadish, K. M.; Smith, K. M.; Guilard, R., Eds, Academic Press: New York, NY, USA, 2003, Vol. 18, pp. 303–349.

7. Thomas, K. E.; Alemayehu, A. B.; Conradie, J.; Beavers, C. M.; Ghosh, A. *Acc. Chem. Res.* **2012**, *45*, 1203–1214.
8. McGown, A. J.; Badiei, Y. M.; Leeladee, P.; Prokop, K. A.; DeBeer, S.; Goldberg, D. P. In *Handbook of Porphyrin Science*; Kadish, K. M.; Smith, K. M.; Guilard, R., Eds. Academic Press: New York, NY, USA, 2011, Vol. 14, pp. 525–599.
9. Aviv, I.; Gross, Z. *Chem. Commun.* **2007**, *20*, 1987–1999.
10. Lemon, C. M.; Dogutan, D. K.; Nocera, D. G. In *Handbook of Porphyrin Science*; K. M.; Smith, K. M.; Guilard, R., Eds. Academic Press: New York, 2011, Vol. 21, pp. 1–143.
11. Simkhovich, L.; Luobeznova, I.; Goldberg, I.; Gross, Z. *Chem. Eur. J.* **2003**, *9*, 201–208.
12. Mahammed, A.; Gray, H. B.; Meier-Callahan, A. E.; Gross, Z. *J. Am. Chem. Soc.* **2003**, *125*, 1162–1163.
13. Simkhovich, L.; Goldberg, I.; Gross, Z. *J. Porphyrins Phthalocyanines* **2002**, *6*, 439–444.
14. Mahammed, A.; Gross, Z. *J. Am. Chem. Soc.* **2005**, *127*, 2883–2887.
15. Gao, Y.; Liu, J.; Wang, M.; Na, Y.; Akermark, B.; Sun, L. *Tetrahedron* **2007**, *63*, 1987–1994.
16. Kadish, K. M.; Fremond, L.; Ou, Z. P.; Shao, J. G.; Shi, C. N.; Anson, F. C.; Burdet, F.; Gros, C. P. ; Barbe, J.-M.; Guilard, R. *J. Am. Chem. Soc.* **2005**, *127*, 5625–5631.
17. Kadish, K. M.; Fremond, L.; Burdet, F.; Barbe, J.-M.; Gros, C. P.; Guilard, R. *J. Inorg. Biochem.* **2006**, *100*, 858–868.
18. Guilard, R.; Jerome, F.; Gros, C. P.; Barbe, J.-M.; Ou, Z. P.; Shao, J. G.; Kadish, K. M. *C. R. Acad. Sci. Series IIC: Chimie* **2001**, *4*, 245–254.
19. Kadish, K. M.; Shao, J. G.; Ou, Z. P.; Fremond, L.; Zhan, R. Q.; Burdet, F.; Barbe, J.-M.; Gros, C. P.; Guilard, R. *Inorg. Chem.* **2005**, *44*, 6744–6754.
20. Collman, J. P.; Kaplun, M.; Decreau, R. A. *Dalton Trans.* **2006**, 554–559.
21. Schechter, A.; Stanevsky, M.; Mahammed, A.; Gross, Z. *Inorg. Chem.* **2012**, *51*, 22–24.
22. Dogutan, D. K.; Stoian, S. A.; McGuire, R.; Schwalbe, M.; Teets, T. S.; Nocera, D. G. *J. Am. Chem. Soc.* **2011**, *133*, 133–140.
23. Kadish, K. M.; Fremond, L.; Shen, J.; Chen, P.; Ohkubo, K.; Fukuzumi, S.; El Ojaimi, M.; Gros, C. P.; Barbe, J.-M.; Guilard, R. *Inorg. Chem.* **2009**, *48*, 2571–2582.
24. Kadish, K. M.; Shen, J.; Fremond, L.; Chen, P.; El Ojaimi, M.; Chkounda, M.; Gros, C. P.; Barbe, J.-M.; Ohkubo, K.; Fukuzumi, S.; et al. *Inorg. Chem.* **2008**, *47*, 6726–6737.
25. Ou, Z. P.; Lu, A. X.; Meng, D. Y.; Huang, S.; Fang, Y. Y.; Lu, G. F.; Kadish, K. M. *Inorg. Chem.* **2012**, *51*, 8890–8896.
26. Schwalbe, M.; Dogutan, D. K.; Stoian, S. A.; Teets, T. S.; Nocera, D. G. *Inorg. Chem.* **2011**, *50*, 1368–1377.
27. Abu-Omar, M. M. *Dalton Trans.* **2011**, *40*, 3435–3444.
28. Will, S.; Lex, J.; Vogel, E.; Adamian, V. A.; Van Caemelbecke, E.; Kadish, K. M. *Inorg. Chem.* **1996**, *35*, 5577–5583.
29. Adamian, V. A.; D'Souza, F.; Licoccia, S.; DI Vona, M. L.; Tassoni, E.; Paolesse, R.; Boschi, T.; Kadish, K. M. *Inorg. Chem.* **1995**, *34*, 532–540.
30. Kadish, K. M.; Adamian, V. A.; Van Caemelbecke, E.; Gueletti, E.; Will, S.; Erben, C.; Vogel, E. *J. Am. Chem. Soc.* **1998**, *120*, 11986–11993.
31. Kadish, K. M.; Koh, W.; Tagliatesta, P.; D'Souza, F.; Paolesse, R.; Licoccia, S.; Boschi, T. *Inorg. Chem.* **1992**, *31*, 2305–2313.
32. Kadish, K. M.; Shao, J. G.; Ou, Z. P.; Gros, C. P.; Bolze, F.; Barbe, J.-M.; Guilard, R. *Inorg. Chem.* **2003**, *42*, 4062–4070.
33. Huang, S.; Fang, Y. Y.; Lü, A. X.; Lu, G. F.; Ou, Z. P.; Kadish, K. M. *J Porphyrins Phthalocyanines* **2012**, *16*, 958–967.

34. Nardis, S.; Stefanelli, M.; Mohite, P.; Pomarico, G.; Tortora, L.; Manowong, M.; Chen, P.; Kadish, K. M.; Fronczek, F. R.; McCandless, G. T.; et al. *Inorg. Chem.* **2012**, *51*, 3910–3920.

35. Van Caemelbecke, E.; Will, S.; Autret, M.; Adamian, V. A.; Lex, J.; Gisselbrecht, J.-P.; Gross, M.; Vogel, E.; Kadish, K. M. *Inorg. Chem.* **1996**, *35*, 184–192.

36. Autret, M.; Will, S.; Van Caemelbecke, E.; Lex, J.; Gisselbrecht, J.-P.; Gross, M.; Vogel, E.; Kadish, K. M. *J. Am. Chem. Soc.* **1994**, *116*, 9141–9149.

37. Shen, J.; El Ojaimi, M.; Chkounda, M.; Gros, C. P.; Barbe, J.-M.; Shao, J. G.; Guilard, R.; Kadish, K. M. *Inorg. Chem.* **2008**, *47*, 7717–7727.

38. Ou, Z. P.; Erben, C.; Autret, M.; Will, S.; Rosen, D.; Lex, J.; Vogel, E.; Kadish, K. M. *J. Porphyrins Phthalocyanines*, **2005**, *9*, 398-412.

39. Huang, H. C.; Shown, I.; Chang, S.T.; Hsu, H. C.; Du, H. Y.; Kuo, M. C.; Wong, K. T.; Wang, S. F.; Wang, C. H.; Chen, L. C.; et al. *Adv. Funct. Mater.* **2012**, *22*, 3500–3508.

40. Steene, E.; Wondimagegn, T.; Ghosh, A. *J. Phys. Chem. B* **2001**, *46*, 11406–11413.

41. Gross, Z. *J. Biol. Inorg. Chem.* **2001**, *6*, 733–738.

42. Cai, S.; Walker, F. A.; Licoccia, S. *Inorg. Chem.* **2000**, *39*, 3466–3478.

43. Bard, A. J.; Faulkner, L. R. *Electrochemical Methods: Fundamentals and Applications*, 2nd ed., John Wiley & Sons, Inc: New York, NY, USA, 2001.

44. Treimer, S.; Tang, A.; Johnson, D. C. *Electroanalysis* **2002**, *14*, 165–171.

45. Shi, C.; Anson, F. C. *Inorg. Chem.* **1998**, *37*, 1037–1043.

46. Sun, B.; Ou, Z. P.; Meng, D. Y.; Fang Y. Y.; Song, Y.; Zhu, W. H.; Solntsev, P. V.; Nemykin, V. N.; Kadish, K. M. *Inorg. Chem.* **2014**, *53*, 8600–8609.

47. Ou, Z. P.; Zhu, J. L.; Lin, W. S.; Fang, Y. Y.; Lu, G. F. *Chem. J. Chinese U.* **2012**, *33*, 1130–1137.

48. Conway, B. E.; Angerstein-Kozlowska, H.; Sharp, W. B. A.; Criddle, E. E. *Anal. Chem.* **1973**, *45*, 1331–1336.

49. Hsueh, K. L.; Conzalez, E. R.; Srinivasan, S. *Electrochim. Acta* **1983**, *28*, 691–697.